Materials Chemistry and Physics 117 (2009) 41–45

Contents lists available at ScienceDirect

Materials Chemistry and Physics

journal homepage: www.elsevier.com/locate/matchemphys

Effects of different carbonate precipitators on $LiNi_{1/3}Co_{1/3}Mn_{1/3}O_2$ morphology and electrochemical performance

Haibo Ren [a], Yanghui Huang [a,b], Yunhong Wang [a], Zhongjing Li [a], Ping Cai [a], Zhenghe Peng [a,*], Yunhong Zhou [a]

[a] Department of Chemistry, Wuhan University, Wuhan 430072, PR China
[b] Department of Applied Chemistry, East China Institute of Technology, Fuzhou 344000, PR China

ARTICLE INFO

Article history:
Received 3 September 2008
Received in revised form 18 December 2008
Accepted 2 January 2009

Keywords:
Composite materials
Sintering
Crystal structure
Electrochemical properties

ABSTRACT

Compounds $LiNi_{1/3}Co_{1/3}Mn_{1/3}O_2$ are prepared by adopting different carbonate, i.e., $NaHCO_3$, NH_4HCO_3 and Na_2CO_3 under the same conditions, which results in the impressive differences in the morphology properties and electrochemical behaviors of $LiNi_{1/3}Co_{1/3}Mn_{1/3}O_2$. The microscopic structural features of $LiNi_{1/3}Co_{1/3}Mn_{1/3}O_2$ are investigated using X-ray diffraction (XRD) and Scanning Electron Microscopy (SEM). The electrochemical properties of $LiNi_{1/3}Co_{1/3}Mn_{1/3}O_2$ are carried out by charge–discharge cycling tests and the electrochemical reactions during charge–discharge process are also investigated by the cyclic voltammetry (CV). Experimental results show that the microscopic structural features, the morphology properties and electrochemical performances are deeply related to the precipitators. In addition, the cyclic voltammetry indicates that the oxidation of nickel occurs by two steps $Ni^{2+} \rightarrow Ni^{3+} \rightarrow Ni^{4+}$.

© 2009 Published by Elsevier B.V.

1. Introduction

Lithium-ion batteries have presently become attractive for portable electronic devices because of their higher output voltage and energy density than other rechargeable systems. Originally, commercial lithium-ion cells employ the layered $LiCoO_2$ cathode, which has a theoretical capacity of 275 mAh g^{-1}. The practically attainable capacity, however, is found to be only 120–130 mAh g^{-1} in the voltage range 2.7–4.2 V [1,2]. To increase the capacity, several cationic substitutions such as $LiNi_{0.8}Co_{0.2}O_2$ [3,4], $LiNi_{0.5}Mn_{0.5}O_2$ [5,6] and $LiNi_{1/3}Co_{1/3}Mn_{1/3}O_2$ [7–12] are being intensively pursued. Especially, computation [13] and XPS [14] studies on $LiNi_{1/3}Co_{1/3}Mn_{1/3}O_2$ show that the predominant oxidation states of Ni, Co, Mn ions are +2, +3, +4, respectively. In such a system, the electrochemical capacity is derived predominantly from redox reactions on the nickel and cobalt ions. The relatively high concentration of inactive Mn^{4+} ions that remains constant throughout charge and discharge is believed to contribute to the enhanced stability and higher reversible capacity of these types of electrodes compared to those containing only cobalt and nickel. Thus, this solid solution could be one of the promising cathode materials. Unfortunately, due to the complicated composition, the cathode properties of $LiNi_{1/3}Co_{1/3}Mn_{1/3}O_2$ should be sensitively dependent on microscopic features like the distribution of transition metal and the particle morphology. As a result, it is difficult to prepare this complicated material, and the rate capability of this material depends on the synthetic route which has greater influence on the particle morphology. Therefore, it is important for $LiNi_{1/3}Co_{1/3}Mn_{1/3}O_2$ to select suitable preparation method. In order to synthesize uniform and homogeneous $LiNi_{1/3}Co_{1/3}Mn_{1/3}O_2$, some research groups have reported hydroxide coprecipitation method [10,15–17]. In fact, in hydroxide coprecipitation method, $Mn(OH)_2$ (Mn^{2+}) oxidizes gradually to MnOOH (Mn^{3+}) or MnO_2 (Mn^{4+}) upon precipitation conditions which can decrease the homogeneity of the final product. Therefore, it is critical to control the valence state of Mn stable in aqueous solution. The carbonate coprecipitation method adopted to prepare the composite precursor could keep valence state of Mn^{2+} stable in aqueous solution during precipitation process so that the homogeneous solid solution could be obtained. In our work, the $NaHCO_3$, NH_4HCO_3 and Na_2CO_3 are all employed as precipitator to yield $LiNi_{1/3}Co_{1/3}Mn_{1/3}O_2$, of which differences in structure, morphology and electrochemical properties are also reported.

2. Experimental

$LiNi_{1/3}Co_{1/3}Mn_{1/3}O_2$ was synthesized by carbonate coprecipitation method. Three of aqueous solutions (50 ml) containing $NiSO_4{\cdot}6H_2O$, $CoSO_4{\cdot}7H_2O$ and $MnSO_4{\cdot}H_2O$ (cationic ratio of Ni:Co:Mn = 1:1:1) with a total metal ion concentration of 0.5 M were dropped into the strongly stirred 50 ml of 1 M $NaHCO_3$, NH_4HCO_3 and Na_2CO_3 solutions at a speed of one drop per second at 80 °C, respectively. After reaction for 10 h, the sediment was filtered with distilled water for several times before being dried at 120 °C for 5 h. The obtained precursor powder was mixed with 6% excess Li_2CO_3 (excess amount of Li salt was used to compensate for possible Li loss during the calcination) by a mortar and the powder was pressed into pellets.

* Corresponding author. Tel.: +86 27 87218254; fax: +86 27 68754067.
E-mail address: pengzh@chem.whu.edu.cn (Z. Peng).

0254-0584/$ – see front matter © 2009 Published by Elsevier B.V.
doi:10.1016/j.matchemphys.2009.01.002

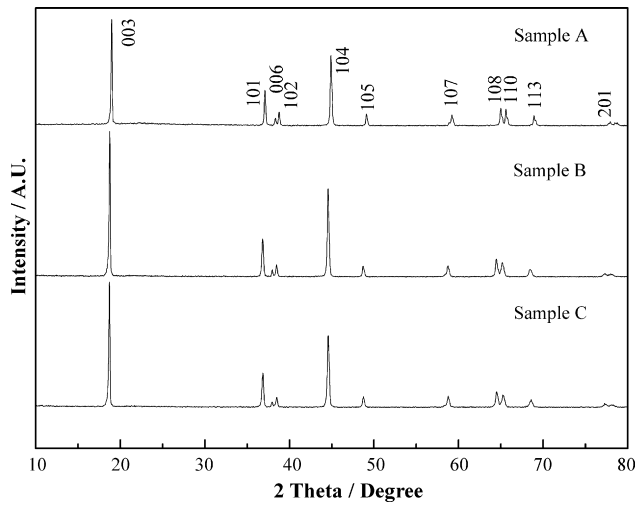

Fig. 1. XRD patterns of $LiNi_{1/3}Co_{1/3}Mn_{1/3}O_2$ prepared from different carbonate.

The pellets were initially heated to 500 °C for 6 h in air and reground later. The pellets were remade and subsequently calcined at 850 °C for 20 h in air to obtain $LiNi_{1/3}Co_{1/3}Mn_{1/3}O_2$. The $LiNi_{1/3}Co_{1/3}Mn_{1/3}O_2$ samples from $NaHCO_3$, NH_4HCO_3 and Na_2CO_3 were denoted as sample A, sample B and sample C, respectively.

X-ray diffraction measurements of the $LiNi_{1/3}Co_{1/3}Mn_{1/3}O_2$ materials were carried out using X-ray diffraction (Shimadzu XRD-6000) with Cu Kα radiation (λ = 1.54056 Å). Lattice parameters and unit-cell volumes were calculated by a least squares method with FullProf Suite program. Particle morphology of the powders after calcination was observed using a scanning electron microscope (SEM, QUANTA-200). Electrochemical charge–discharge experiments were performed using the CR2016 coin-type cell. Test cathode electrodes were prepared by mix 80:15:5 (mass ratio) of active material, acetylene black and PTFE binder, respectively, in isopropyl alcohol. The test cells were assembled with the electrode prepared above as cathode, lithium metal as anode, and Celgard 2300 film as separator in an argon-filled glove box. The electrolyte was 1 M $LiPF_6$ dissolved in EC + DMC (1:1 volume ratio). Cyclic voltammetry (CV) experiments were carried out at a scanning rate 0.1 mV s^{-1} between 2.8 and 4.8 V versus Li/Li^+. All tests were performed at room temperature.

3. Results and discussion

Fig. 1 illustrates the powder X-ray diffraction patterns of the samples A, B and C. The XRD patterns of all samples could be indexed based on the α-$NaFeO_2$ structure (space group: $R\bar{3}m$) without any impurity peaks. The lattice parameters of the samples were calculated by least square method using 10-diffraction lines. The determined parameters are summarized in Table 1. The lattice parameters are somewhat different for the samples. The sample A shows the smallest lattice parameter *a* and the biggest lattice parameter *c*, thus it holds a larger triangle distortion, *c*/*a*. In addition, the three samples have smaller lattice parameters, *a* and *c* compared to those reported [14,18] while a larger triangle distortion, *c*/*a*, but it is similar to some results of Reddy et al. [19,20]. Reddy et al. [19] considered these smaller lattice parameters might be due to smaller cation mixing and better ordering of the transition metal ions in the metal-layer. Hwang et al. [21] believed that the intensity ratio of the (0 0 3) and (1 0 4) peaks ($I_{(003)}/I_{(104)}$) could be used to identify the cation mixing degree. Generally, when the value of intensity ratio is more than 1.2, the cation mixing is small with good layered structure and the higher value indicates lower cation mixing. According to Table 1, the intensity ratios of the sample A, B and C are 1.74, 1.62 and 1.60, respectively. The sample A prepared by $NaHCO_3$ shows the highest structural integrity, i.e., lower cation mixing, whereas the sample C by Na_2CO_3 shows the lowest one. After making a comparison of the values of *c*/*a* and those of $I_{(003)}/I_{(104)}$, it could be guessed that the sample A should have the best crystal structure and will show better electrochemical properties.

Table 1
Lattice parameters of $LiNi_{1/3}$ $Co_{1/3}Mn_{1/3}O_2$ prepared by different carbonate.

Samples	*a* (Å)	*c* (Å)	*c*/*a*	$I_{(003)}/I_{(104)}$
A	2.8478	14.1794	4.98	1.74
B	2.8485	14.1552	4.97	1.62
C	2.8542	14.1759	4.97	1.60
Literature [10]	2.864	14.233	4.969	0.8
Literature [13]	2.867	14.246	4. 969	–
Literature [14]	2.8467	14.1967	4.99	1.6
Literature [15]	2.8496	14.2045	4.98	1.87

Normally, the crystal structure and morphology are two main factors which affect the electrochemical performance of the materials. Fig. 2 shows the SEM micrographs of the three samples with different magnifications. The powder of the sample A and B is quasi-spherical secondary particle formed by the primary particle (<1 μm) aggregating each other. This kind of morphology could be thought to enhance high rate capability with respect to high surface area without decreasing of tapping density [22]. From Fig. 2a and c, we can see that the particle size of the sample A has a better consistency than that of the sample B. The uniform distribution leads to the uniform depth of charge (DOC) of each particle, which increases the utilization of the material to enhance the overall battery performances. The powder of the sample C is formed by the primary particle, but these small particles are aggregated into irregular shapes. We think that this kind of morphology does not benefit its electrochemical performance.

Testing cells are firstly operated at a current density of 50 mA g^{-1} in the voltage range of 3–4.3 V. The initial charge–discharge curves of the three samples are presented in Fig. 3, and their cycling performances under this condition are offered in Fig. 4. As shown in Fig. 3, the first charge/discharge specific capacities are 187.6/166.6, 189.8/164.3 and 188.8/162.9 mAh g^{-1} with a coulombic efficiency about 88.8%, 86.6% and 86.3% for samples A, B and C, respectively. All cells show coulombic inefficiencies; i.e., more capacity is observed upon charge than on discharge. The irreversible capacity loss might be attributed to the formation of a solid electrolyte interface (SEI) on the surface of the electrode and insufficient soaking of the electrode material during the first cycle [23]. Moreover, we can also find from Fig. 3 that the polarization degree of the electrode composed of sample A, B and C exists difference in charge/discharge process. The electrode composed of the sample A shows a lower polarization and the electrode composed of the sample C has a higher polarization, which may be one of the reasons leading to the different charge/discharge capacities. According to Fig. 4, at the end of the 30th cycle, the retained discharge capacities for the sample A, B and C are 158.8, 153.6 and 151.6 mAh g^{-1}, respectively, which are 95.3%, 93.5% and 93.1% of initial discharge capacity.

Obviously, the sample A synthesized from $NaHCO_3$ reveals excellent electrochemical performance. The sample C, However, synthesized from Na_2CO_3 shows poor electrochemical properties. These results are consistent with the analysis of XRD and SEM.

$LiNi_{1/3}Co_{1/3}Mn_{1/3}O_2$ is only partially de-intercalated and intercalated when cells are charged and discharged in the voltage range of 3–4.3 V. Higher discharge capacities can be obtained when the voltage range is broadened, but the increased coulombic inefficiencies and more rapid capacity fading will be brought. To illustrate these phenomena and show the differences of the three samples operated in broader voltage, the voltage range 2.5–4.6 V (50 mA g^{-1}) is adopted. Here, 4.6 V is chosen as the upper limit because the critical upper limit of $LiNiO_2$ and $LiCoO_2$ is 4.6 V [18,24]. Fig. 5 shows the cycling performance of the sample A, B and C under given conditions and Table 2 also gives some data about the charge–discharge capacities, coulombic efficiency and capacity retention rations of the three samples under the same conditions. For comparison pur-

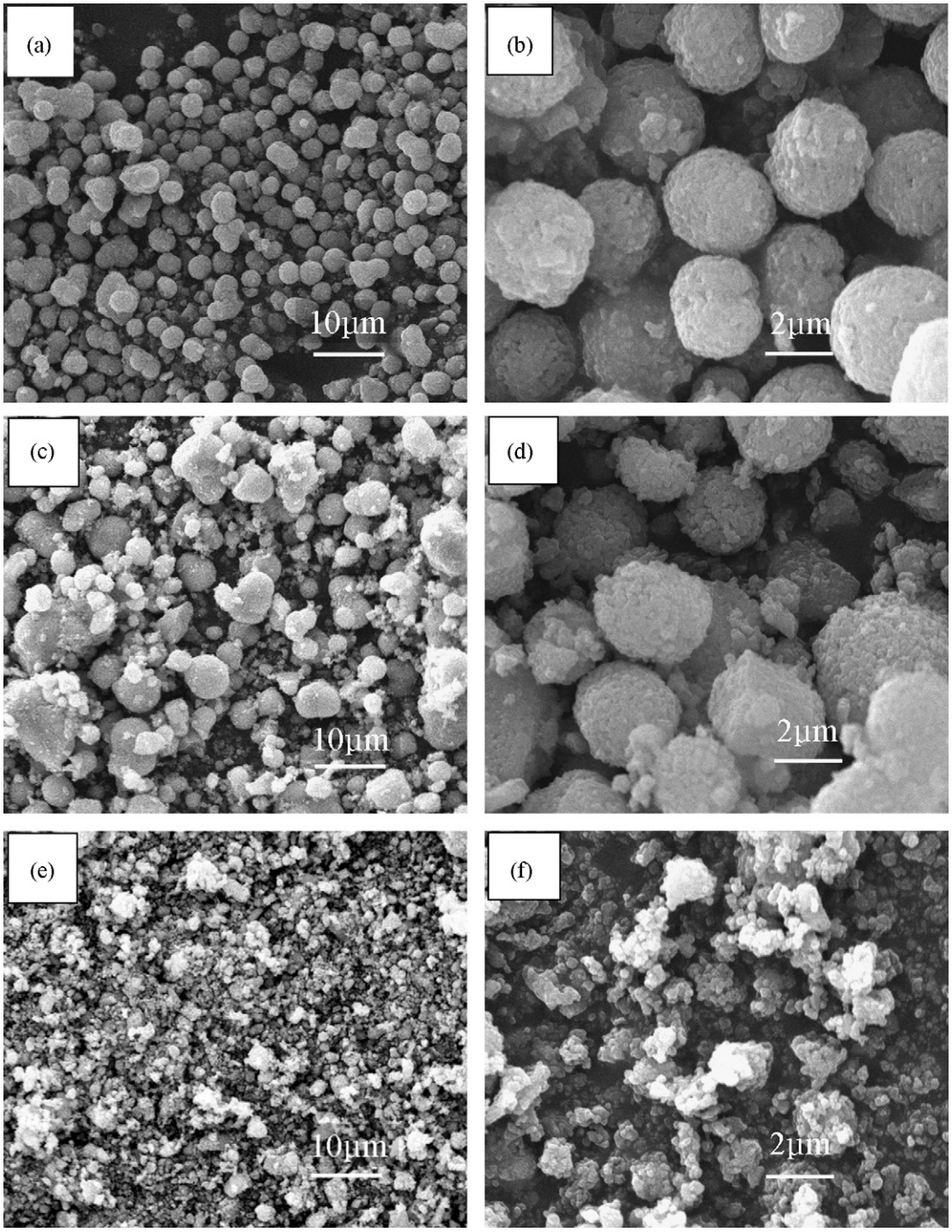

Fig. 2. SEM micrographs of $LiNi_{1/3}Co_{1/3}Mn_{1/3}O_2$ prepared from different carbonate. (a and b) The sample A; (c and d) the sample B; (e and f) the sample C.

Table 2
The charge–discharge data for the samples A, B and C in the voltage range of 2.5–4.6 V.

Samples	1st cycle Q_{charge} (mAh g^{-1})	1st cycle $Q_{discharge}$ (mAh g^{-1})	1st cycle coulombic efficiency (%)		30th cycle $Q_{discharge}$ (mAh g^{-1})	30th cycle capacity retention (%)	
			2.5–4.6 V	3–4.3 V		2.5–4.6 V	3–4.3 V
A	228.4	200.5	87.8	88.8	177.0	88.3	95.3
B	228.9	196.2	85.7	86.6	175.2	89.3	93.5
C	230.1	193.8	84.2	86.3	158.1	81.6	93.1

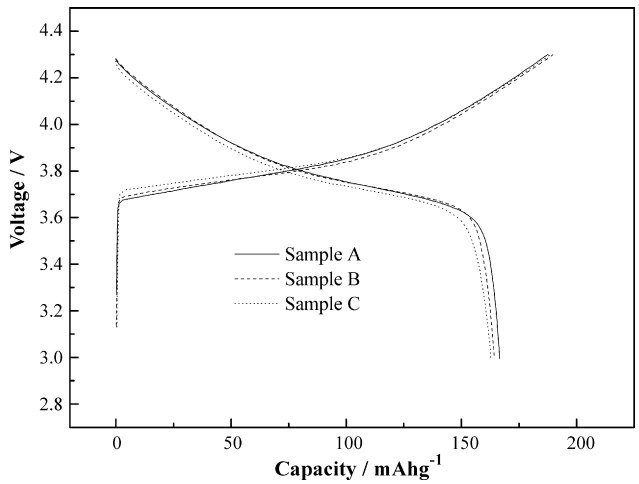

Fig. 3. Initial charge–discharge curves of the three samples operated in the voltages range of 3–4.3 V under a current density 50 mA g^{-1}.

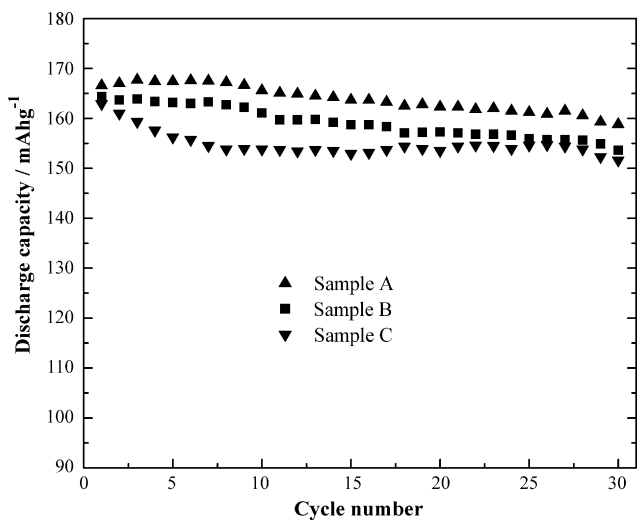

Fig. 4. Specific discharge capacity as a function of cycle number for the samples operated in the voltage range of 3–4.3 V under a current density 50 mA g^{-1}.

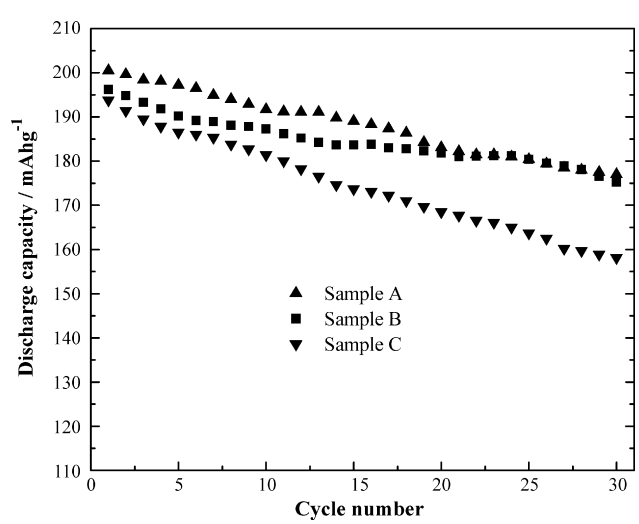

Fig. 5. Specific discharge capacity as a function of cycle number for the samples operated in the voltage range of 2.5–4.6 V under a current density 50 mA g^{-1}.

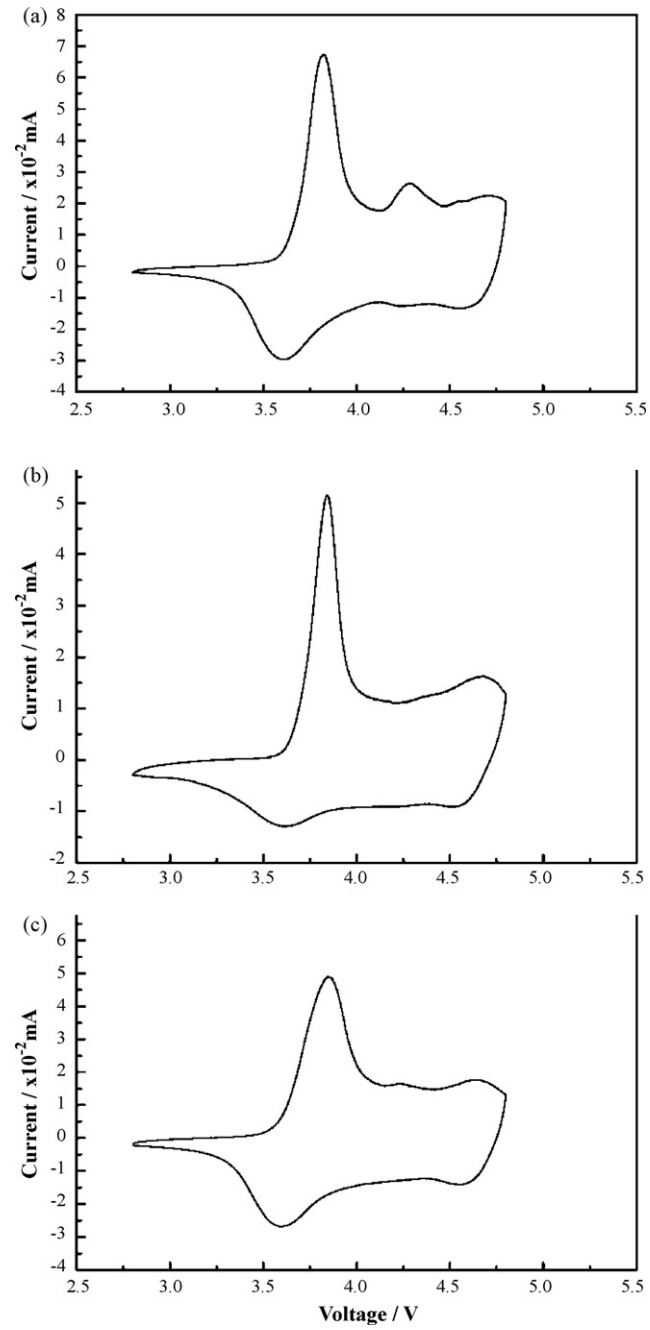

Fig. 6. CV curves of the three samples. (a) The sample A; (b) the sample B; (c) the sample C.

poses, some data from the narrower voltage range are also listed in Table 2. From the table, we can find that the initial discharge capacities for the three samples are remarkably increased. However, their coulombic efficiencies decrease and the speed of capacity fading increases. In addition, from Figs. 4 and 5, it is noticed that the sample C has different cycling characters under the different voltage range. The discharge capacity experiences three stages, which are decline, stability and decline again under the narrower voltage range. However, the discharge capacity descends linearly without a stable stage under the broader voltage range. These phenomena indicate that the different charge–discharge voltage range may have different influence on the electrochemical performances of electrode material. Essentially, it should be attributed to the different changes of microstructure under the different charge–discharge voltage range.

We carry out cyclic voltammetry to monitor the electrochemical reactions during charge–discharge process as shown in Fig. 6. Fig. 6a–c shows only the first cycle curves of the sample A, B and C, respectively. All the three samples show the two anodic peaks at 3.6–3.9 and 4.6–4.8 V whereas the corresponding cathodic peak is at 3.5–3.8 and 4.5–4.7 V. They are ascribed to Ni^{2+}/Ni^{4+} and Co^{3+}/Co^{4+} redox couples [14], respectively. However, an anodic peak, around 3.9–4.4 V, can be obviously observed in Fig. 6a and c. It should be assigned as the oxidation of $Ni^{3+} \rightarrow Ni^{4+}$ [25,26]. So we think the oxidation of nickel occurs by two steps $Ni^{2+} \rightarrow Ni^{3+} \rightarrow Ni^{4+}$ rather than in a single step $Ni^{2+} \rightarrow Ni^{4+}$. Each oxidation process in charge process could be assigned as $Ni^{2+/3+}$ (3.6–3.9 V) [20,21], $Ni^{3+/4+}$ (3.9–4.4 V) and $Co^{3+/4+}$ (4.6–4.8 V), respectively.

4. Conclusions

Layered compounds $LiNi_{1/3}Co_{1/3}Mn_{1/3}O_2$ are prepared by different carbonate coprecipitation methods, which results in the differences in morphology and microstructure by the SEM observation and the XRD experiment. The electrochemical tests show that compound $LiNi_{1/3}Co_{1/3}Mn_{1/3}O_2$ synthesized from $NaHCO_3$ holds the higher initial discharge capacities of 166.6 mAh g^{-1} (3–4.3 V, 50 mA g^{-1}) and 200.5 mAh g^{-1} (2.5–4.6 V, 50 mA g^{-1}), as well as good cycling performance, which are superior to those of the materials from NH_4HCO_3 and Na_2CO_3. Cyclic voltammetry results show the oxidation of nickel occurs by two steps $Ni^{2+} \rightarrow Ni^{3+} \rightarrow Ni^{4+}$ rather than in a single step $Ni^{2+} \rightarrow Ni^{4+}$.

Acknowledgement

We gratefully acknowledge the financial support from the National Nature Science Foundation of China (No. 29833090, No. 29771025 and No. 20573078).

References

[1] A. Manthiram, J. Kim, Chem. Mater. 10 (1998) 2895–2909.
[2] J. Fan, P.S. Fedkiw, J. Power Sources 72 (1998) 165–173.
[3] G.T.K. Fey, R.F. Shiu, V. Subramanian, J.G. Chen, C.L. Chen, J. Power Sources 103 (2002) 265–272.
[4] S.B. Yi, H.T. Chung, H.G. Kim, Electrochem. Commun. 9 (2007) 591–595.
[5] D.H. Park, S.T. Lim, S.J. Hwang, C.S. Yoon, Y.K. Sun, J.H. Choy, Adv. Mater. 17 (2005) 2834–2837.
[6] Y. Hinuma, Y.S. Meng, K. Kang, G. Ceder, Chem. Mater. 19 (2007) 1790–1800.
[7] H. Ren, Y. Wang, D. Li, L. Ren, Z. Peng, Y. Zhou, J. Power Sources 178 (2008) 439–444.
[8] S. Venkatraman, J. Choi, A. Manthiram, Electrochem. Commun. 6 (2004) 832–837.
[9] J. Li, J.M. Zheng, Y. Yang, J. Electrochem. Soc. 154 (2007) A427–A432.
[10] C. Deng, L. Liu, W. Zhou, K. Sun, D. Sun, Electrochim. Acta 53 (2008) 2441–2447.
[11] P. Reale, D. Privitera, S. Panero, B. Scrosati, Solid State Ion. 178 (2007) 1390–1397.
[12] H.Y. Chang, C.L. Sheu, S.Y. Cheng, J. Power Sources 174 (2007) 985–989.
[13] B.J. Hwang, Y.W. Tsai, D. Carlier, G. Ceder, Chem. Mater. 15 (2003) 3676–3682.
[14] K.M. Shaju, G.V. Subba Rao, B.V.R. Chowdari, Electrochim. Acta 48 (2002) 145–151.
[15] B. Lin, Z. Wen, Z. Gua, S. Huang, J. Power Sources 175 (2008) 564–569.
[16] X. Luo, X. Wang, L. Liao, S. Gamboa, P.J. Sebastian, J. Power Sources 158 (2006) 654–658.
[17] S. Zhang, Electrochim. Acta 52 (2007) 7337–7342.
[18] T. Ohzuku, Y. Makimura, Chem. Lett. 7 (2001) 642–643.
[19] M.V. Reddy, G.V. Subba Rao, B.V.R. Chowdari, J. Power Sources 159 (2006) 263–267.
[20] J. Guo, L.F. Jiao, H.T. Yuan, H.X. Li, M. Zhang, Y.M. Wang, Electrochim. Acta 51 (2006) 3731–3735.
[21] B.J. Hwang, R. Santhanam, C.H. Chen, J. Power Sources 114 (2003) 244–252.
[22] T.H. Cho, S.M. Park, M. Yoshio, T. Hiraib, Y. Hideshima, J. Power Sources 142 (2005) 306–312.
[23] Z. Wang, Y. Sun, L. Chen, X. Huang, J. Electrochem. Soc. 151 (2004) A914–A921.
[24] J.M. Paulsen, C.L. Thomas, J.R. Dahn, J. Electrochem. Soc. 147 (2000) 861–868.
[25] J. Reed, G. Ceder, Electrochem. Solid State Lett. 5 (2002) A145–A148.
[26] Y.S. Hong, Y.J. Park, K.S. Ryu, S.H. Chang, Y.J. Shin, J. Power Sources 147 (2005) 214–219.